Mechanical properties of carbon foams under quasi-static and dynamic loading

Zhejian Li, Wensu Chen*, Hong Hao*

Centre for Infrastructural Monitoring and Protection

School of Civil and Mechanical Engineering, Curtin University, Australia

*corresponding authors: wensu.chen@curtin.edu.au; hong.hao@curtin.edu.au

Abstract

In this study, compressive behaviours of carbon foam are investigated experimentally under quasi-static and dynamic loading. Carbon foams with two densities of 320 and 480 kg/m^3 are considered and their microstructures are compared. Two testing machines are employed to apply quasi-static and dynamic compressive load respectively with the strain rate varying between 6.67×10^{-4} s^{-1} and 178 s^{-1}. The mechanical properties of carbon foams including compressive strength and modulus are measured under various strain rates and their dynamic increase factors (DIF) are compared. Based on the testing data, empirical formulae are proposed for both types of carbon foams to predict their dynamic mechanical properties, i.e., compressive strength and modulus.

Keywords: Carbon foam; dynamic crushing; compressive strength

1 Introduction

Cellular materials are widely used in many applications due to their lightweight and high strength characteristics. Different topologies of the cellular material including lattices [1-3], honeycomb [4-6] and corrugated structures [7, 8] have been extensively investigated. Despite high strength to weight ratio, some of these common cellular structures [5, 8] have inconsistent crushing resistance under large deformation, making them non-ideal for the applications as energy absorbers. Foam materials on the other hand, often have low initial crushing resistance and are capable of undergoing large deformation [9]. Mechanical properties of these foam materials including polymer foams [10, 11], syntactic foams [12-15] and metallic foams [16-18] were studied under various loading conditions. Foam materials were also used as filler inside the structures such as tubes and panels to significantly enhance their structural mechanical properties owing to the foam-wall interaction effect [19]. Strain rate effect on mechanical properties of foam materials was extensively studied under quasi-static and dynamic loading. Many foam materials including EPS foam [10, 11], and closed-cell aluminium foams [20] show different levels of strain rate sensitivity. Very low strain rate sensitivity has been observed on PU foams [11] and some aluminium foams up to strain rate nearly 3000 s^{-1} [9].

Carbon foams have drawn attention in recent years due to their thermal, mechanical and electromagnetic characteristics [21]. Different applications of carbon foam were studied. The electromagnetic shielding performance of carbon foams was investigated as well [21]. Due to their low thermal conductivity and lightweight, carbon foams can be used as thermal protection on spacecraft for its re-entry to the earth's atmosphere [22]. Hypervelocity impact resistance of reinforced carbon-carbon composite with carbon foam backing at high temperature was investigated [22]. Quasi-static compressive stress-strain response of cellular vitreous carbon foam (CVC) and reticulated vitreous carbon foam (RVC) was studied as well recently [23]. The carbon foam with a plate glued on both ends of specimens has the modulus almost 10 times than the specimen without a plate. Effects of cell size and material density on mechanical behaviours of the carbon foams were also studied. However, only quasi-static tests on carbon foams were carried out.

As a new form of cellular foam with low density, high operational temperature, and high corrosive resistance [24], carbon foam has potential to be used as composite structure for impact mitigation or energy absorption under some harsh conditions such as high temperature or high corrosive environment where conventional metal or polymeric composite structures might deteriorate quickly. However, there is no research on the dynamic behaviour of carbon foams in open literature yet. Therefore, to better design carbon foam composite structures to resist dynamic loads, it is necessary to understand the mechanical properties of carbon foams under dynamic loading conditions.

In this study, the mechanical properties of carbon foams with two densities are investigated under various strain rates (from 6.67×10^{-4} to 178 s^{-1}). Shimadzu uniaxial testing machine is used for quasi-static and low speed crushing test for up to 5 mm/s. Instron testing machine is used for intermediate crushing speeds from 0.2 m/s to 10 m/s. Compressive strength and secant modulus of two carbon foams are recorded and analyzed under these strain rates. The dynamic increase factors (DIF) of the carbon foams with two densities are calculated and empirical formulae of the mechanical properties such as compressive strength and modulus are derived with respect to strain rate as well.

2 Carbon foam specimens

2.1 Specimen preparation

Two types of coal-based carbon foams CFOAM320 and CFOAM480 used in this study have the marked densities of 320 and 480 kg/m^3 respectively. CFOAM® is a trademark owned by CFOAM LLC and the foam panels were procured from CFOAM LLC. The carbon foam panels with a thickness of 50 mm were cut into cylindrical specimens for material testing. Each has a diameter of 75 mm and a height of 50 mm as shown in Figure 1 (a).

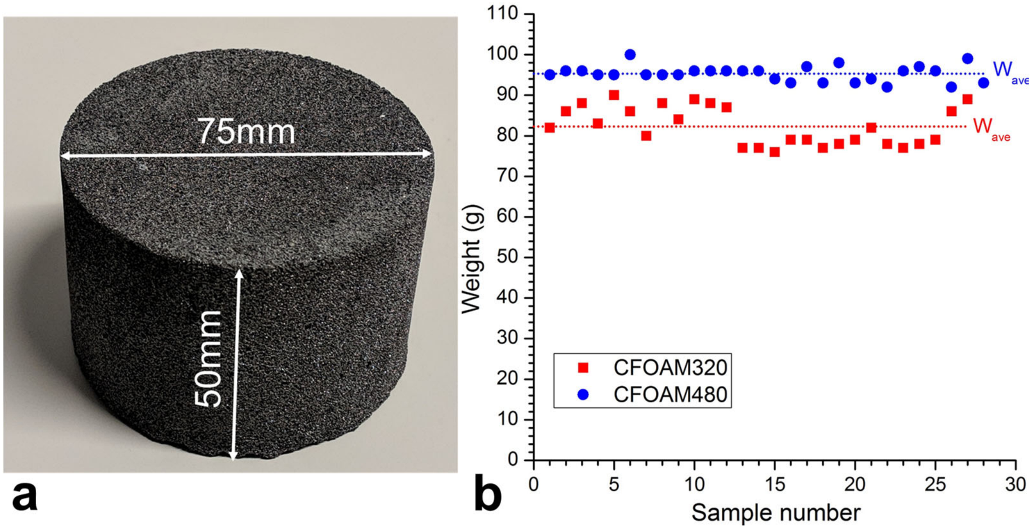

Figure 1. (a) Specimen of carbon foam; (b) scatter chart of weight for two types of carbon foams with an average weight marked out

A total of 55 specimens of two densities were prepared. The weight of each specimen is measured. The weight distributions of the two carbon foam specimens are shown in Figure 1 (b). The weights of carbon foam specimens are listed in Table 1. CFOAM320 has a larger variation in terms of the mass of specimens, where a standard deviation of 4.681 g is calculated as compared to 1.926 g for CFOAM480. The average densities of these two carbon foams are calculated using average specimen mass divided by volume. As listed in Table 1, the average bulk density of CFOAM320 specimens is 371 kg/m^3, larger than the given density of 320 kg/m^3 by the supplier. The average bulk density of CFOAM480 specimens is 432 kg/m^3, slightly smaller than the designated density of 480 kg/m^3. It should be noted that similar variation in densities can be observed for closed-cell aluminium foam [25].

Foam type	Average specimen weight (g)	Median specimen weight (g)	Standard deviation (g)	Calculated density (g/cm^3)
CFOAM320	82.30	82.0	4.681	0.371
CFOAM480	95.32	95.5	1.926	0.432

Table 1. Weight and density of two carbon foam specimens

A classic micromechanical model of open-cell aluminium foam material has been developed by Gibson and Ashby [26], which predicts the fracture of foams by the successive failure of bending in the struts. The plastic yield stress, σ_{pl} is a function of the relative density of the open-cell foam material as follows,

$$\frac{\sigma_{pl}}{\sigma_{ys}} \approx 0.3\left(\frac{\rho}{\rho_0}\right)^{\frac{3}{2}} \tag{1}$$

where σ_{ys} is the static yield strength of base material of the foam, ρ is the density of the foam, and ρ_0 is the density of the solid from which the foam is made.

Based on the model of closed cell aluminium foam [27], $\frac{\sigma_{pl}}{\sigma_{ys}}$ of the foam material incorporating strain rate effect can be expressed as follows:

$$\frac{\sigma_{pl}}{\sigma_{ys}} = x(1+y\left(\frac{\dot{\varepsilon}}{\dot{\varepsilon}_0}\right)^z)\left(\frac{\rho}{\rho_0}\right)^w \tag{2}$$

where *x, y, z*, and *w* are coefficients and dimensionless, $\dot{\varepsilon}$, $\dot{\varepsilon}_0$ is dynamic and quasi-static strain rate with the unit of s^{-1} , respectively.

2.2 Microstructure comparison

Figure 2 shows the Scanning Electron Microscopic (SEM) images of CFOAM320 and CFOAM480 under the magnifications of 15 times, 30 times and 100 times, captured by Zeiss NEON 40 EsB high resolution dual beam scanning electron microscope. Both carbon foams are closed-cell structure with some of the pores interconnected with adjacent pores. The difference in pore size, connectivity and regularity of the pores can be observed between two carbon foams. As compared to CFOAM480, CFOAM320 has a larger average pore size with slightly more regular sizes and shapes of the pores. It has slightly lower connectivity of the pores, as less interconnected pores are observed for CFOAM320. It is worth noting that the microstructures of both carbon foams are different from vitreous carbon foams investigated in the previous studies [21, 23, 28]. Regular 3D arrangement of tetrahedral open-cell microstructures is observed for reticulated vitreous carbon foams [21, 23, 28]. The heat-treated mesophase-pitch-derived carbon foams have similar microstructures to the carbon foams used in this study, where spherical microstructures with interconnected pores are shown between most of the cells [28]. However, less layering of the cells is shown in this study, which results in smoother cell walls comparing to mesophase-pitch-derived carbon foams [28].

Comparisons of the pore of CFOAM320 and CFOAM480 are shown in Figure 2 (e, f). The pore size and cell thickness are measured for both carbon foams. A typical pore length of CFOAM320 is about 640 μm as shown in Figure 2 (e), almost twice than that of CFOAM480 with a typical pore size around 280 to 334 μm. The cell wall thickness is slightly different as well for these two carbon foams. CFOAM480 has a slightly larger cell wall thickness at the middle of the pore than CFOAM320. However, it should be noted that the cell walls for both foams are not uniform, and the thickness varies along the cell wall. The portion of the cell wall near the interconnected pores is much thinner as marked out in Figure 2 (f).

Some research suggested that the cell size had an insignificant influence on the mechanical properties of foam materials such as plastic collapse strength and Young's modulus, providing the densities of the foams are the same [29]. However, the aspect ratio between specimen size and pore size affects the crushing resistance for both open and closed-cell aluminium foams. When the specimen size is relatively small as compared to the pore size (i.e. < 10 times), the compressive strength and Young's modulus measured could be very different from the properties measured with larger size specimens [25, 30]. For small specimens (specimen size less than 10 times of pore size), larger pore size reduces the compressive strength of foam materials even the densities are the same. This is due to the decreased constraint at the free surface of the foam providing a less stiff boundary layer and the area fraction of cut cell wall at specimen boundary is higher for small specimens [25]. Other research suggested that larger cell size leads to higher compressive strength for open-cell aluminium foam which could be related to a change in the aspect ratio of wall thickness against edge length [31]. Similar edge effect was shown for carbon foams, therefore, some researchers suggest that a minimum of 20 cells are required in all directions of specimen dimension to eliminate the corresponding test errors [23].

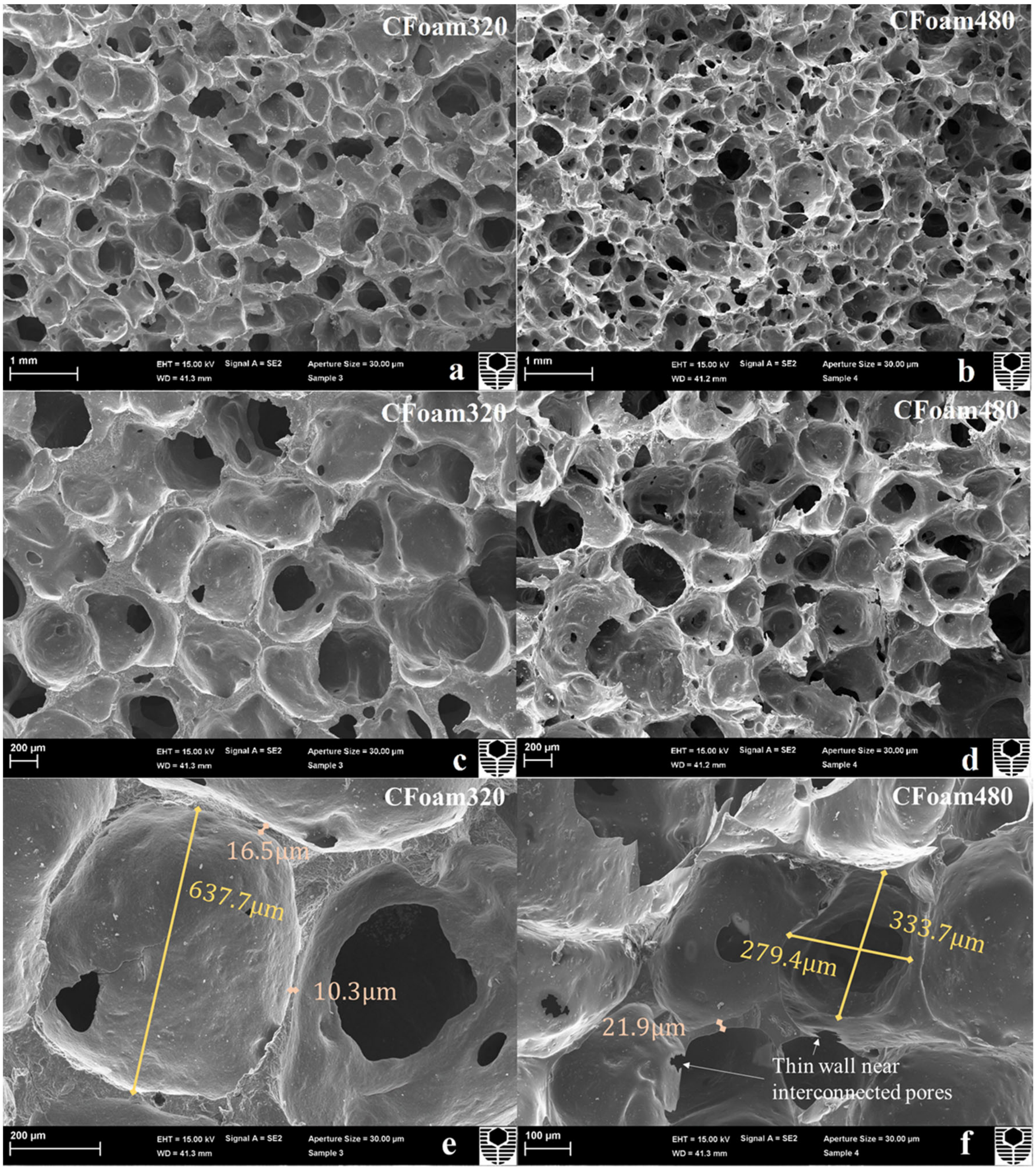

Figure 2. SEM images of carbon foam surface for (a) carbon foam 320 with 15 times magnification; (b) carbon foam 480 with 15 times magnification; (c) carbon foam 320 with 30 times magnification; (d) carbon foam 480 with 30 times magnification; (e) carbon foam 320 with 100 times magnification; (f) carbon foam 480 with 100 times magnification

Since the specimen dimensions used in this study (DIA75×50 mm) are much greater than pore size (around 0.3-0.6 mm), the edge effect may be neglected, which is similar to closed-cell aluminium foams. The difference in density may be the main factor influencing the variations of the mechanical properties of these two foams, similar to other foam materials [26]. Pore size could be another factor as the increase of average cell size broadens the distribution of flaw size within the structure, which controls the fracture of brittle material, and leads to the growth of larger cracks and lower the collapsing stress [23].

3 Crushing test set-up

3.1 Quasi-static and low speed crushing

Shimadzu uniaxial testing machine was used for quasi-static and low speed crushing tests of carbon foams. The testing machine has a speed ranging from 0.001 to 500 mm/min. Three speeds, 2 mm/min, 2.5 mm/s, and 5 mm/s were tested, which corresponds to the expected strain rates of 6.67e^{-4}, 0.05, and 0.1 s^{-1}, respectively. The carbon foam specimens are placed between cylindrical cross-head and base support.

3.2 Intermediate loading rate

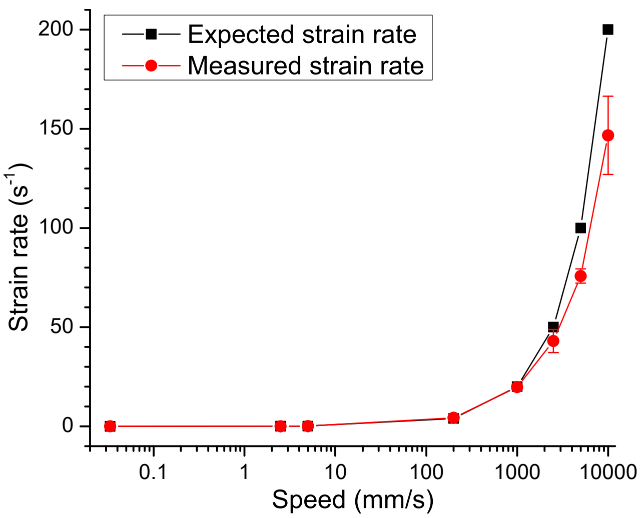

Figure 3. Expected strain rate and measured strain rate at different crushing speeds

High speed testing machine was used for compressive tests of the carbon foams under intermediate loading rates. The carbon foams were crushed under four speeds, 0.2, 1, 5, and 10 m/s, which correspond to the expected strain rate of 4, 20, 100 and 200 s^{-1}. The Instron testing machine is designed to provide a constant moving speed of the crush head throughout the crushing process. However, the speed of cross-head must decelerate to zero before reaching the base support. Therefore, the crushing process throughout each test is not necessarily constant, especially under the higher crushing speed, as a longer distance is required for crushing head to decelerate. Furthermore, as the specimens tested in this study are only 50 mm high, the cross-head has fallen into the decelerating stage for higher crushing rate. Thus, the desired crushing speed and strain rate may not be achieved in the tests at high crushing speeds.

The actual strain rates are measured at the moment of specimens reaching their peak compressive stresses and are shown in Figure 3.

3.3 Stress equilibrium for dynamic testing

It is essential to check the stress equilibrium of the specimen for material testing, which ensures the stress transmitting inside the specimen is uniform [32]. For quasi-static and low speed impact, the stress state equilibrium can be achieved easily, as the stress wave travelling speed is much faster as compared to loading speed. For high speed dynamic material testing, the stress equilibrium should be checked carefully, especially for brittle materials, which may fail at small strains. In general, to achieve this equilibrium state, the elastic stress wave shall be reflected back and forth a few times along the length of the specimen before the failure takes place [32, 33]. The elastic stress wave speed, *c*, can be determined as follows:

$$c = \sqrt{\frac{E}{\rho}} \tag{3}$$

where *E* is the initial elastic modulus of the material and ρ is its density.

4 Results and discussions

4.1 Damage modes

Damage modes of two carbon foams under dynamic crushing are compared. Two different damage modes are observed under 0.2 and 10 m/s crushing. Under 0.2 m/s crushing, damage initiates from both the impacting end and base support at the moment of impact as shown in Figure 4 (a, c). The specimen shatters and splashes near both ends, where the middle portion remains undamaged. The fragments are small and dust-like under 0.2 m/s impact. At the later stage of the crushing, after the peak stress is reached, the damage propagates towards the centre from both ends. Cracks and flying-off of the fragments result in the loss of crushing resistance of the specimen. Under 10 m/s impact, the damage mode is different from that under 0.2 m/s crushing. At the moment of impact, minor damage occurs at both the impacting end and base support, and the small-sized fragments, less than those under 0.2 m/s impact, are generated. This is followed by damage at the base end as shown in Figure 4 (d), while almost no damage is observed at the top impacting end, different from the case under 0.2 m/s impacting as shown in Figure 4 (c). These cracks keep propagating upwards from the lower base end and result in larger fragments flying out from specimen as shown in Figure 4 (f). To more clearly illustrate the above damage modes, a schematic diagram is shown in Figure 5, comparing two damage modes under 0.2 m/s and 10 m/s impact speeds. With the development of these larger cracks under 10 m/s impact, after reaching the peak stress, the crushing resistance of carbon foam reduces quicker than that impacted under lower speeds, as shown in stress-strain curves of section 4.2.

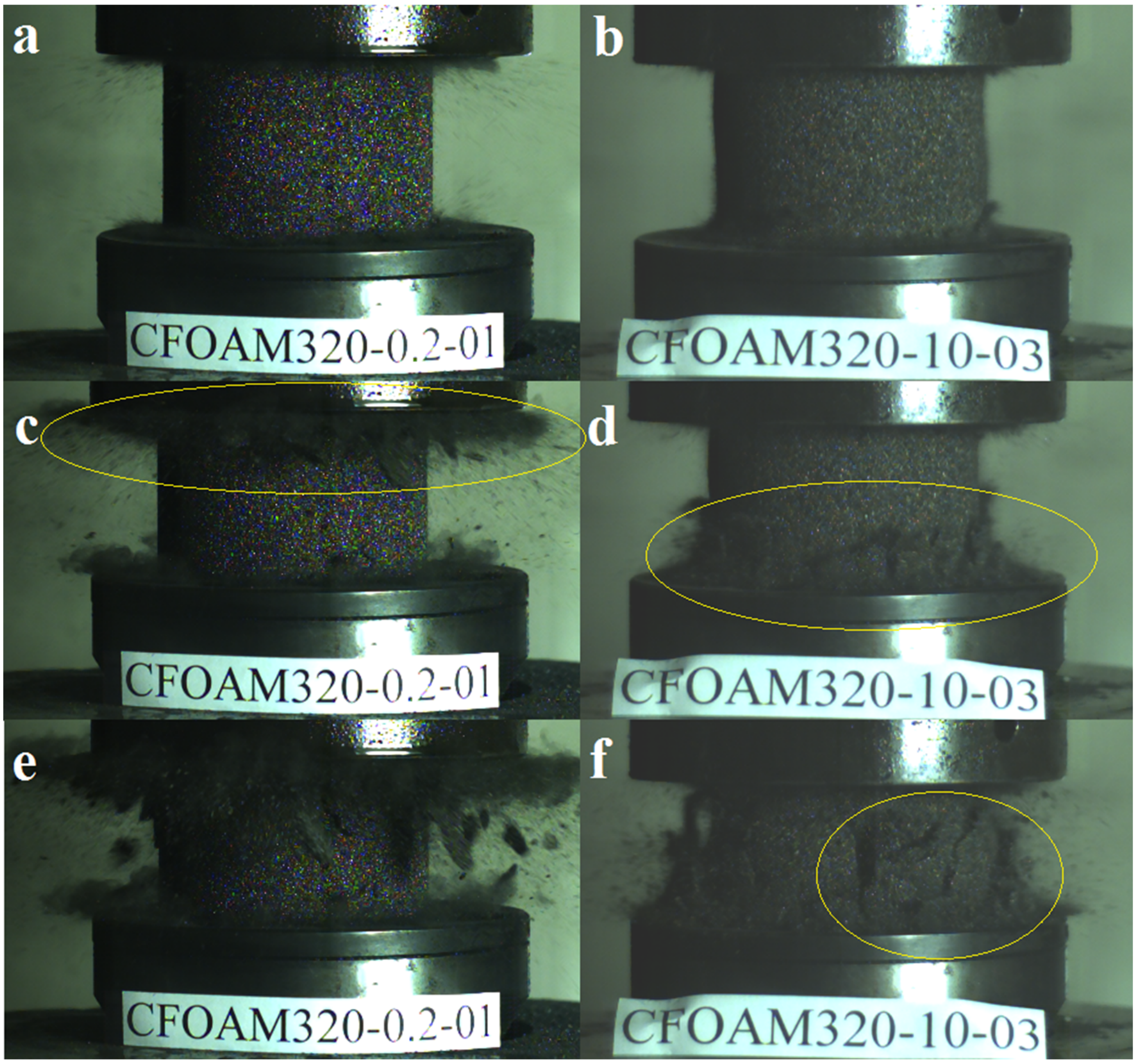

Figure 4. Damage process of carbon foam 320 at different stages under (a, c, e) 0.2 m/s; and (b, d, f) 10 m/s impacting

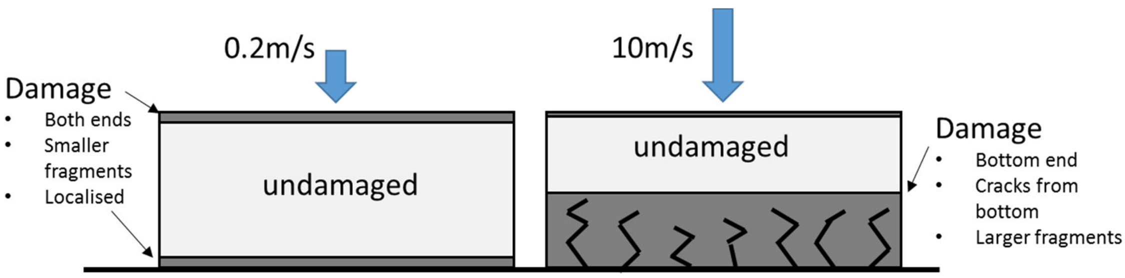

Figure 5. Schematic diagram of two damage modes of carbon foams under 0.2 and 10 m/s impacting

In some cases, large longitudinal cracks occur as marked out in Figure 6 after reaching the peak stress, which results in large pieces flying off the specimen. This sudden loss of large chunks of material from the specimen induces the sudden and significant reduction of crushing resistance. Otherwise, a slower reduction in crushing resistance is expected. For instance, as shown in Figure 6, out of three crushing tests for CFOAM480 under 0.2 m/s, two of which have long cracks along the longitudinal direction of the specimen after reaching the peak stress, and significant stress reductions can be observed at around 0.05 strain. These two types of damage modes occur randomly during the tests for all crushing speeds. As can be observed in Figure 9 and Figure 10, overall, the occurrence of sudden and substantial reductions of crushing stress is observed in less number of tested specimens than the gradual reduction of stress after reaching the maximum in the stress-strain curves. These cracks may be caused by pre-existing defects throughout the height of the specimen. It is worth noting that these long longitudinal cracks only reduces the crushing resistance for a short period of time, with further crushing, the cracked parts provide some resistance once it is again in contact with the rest of the specimen or with the crosshead.

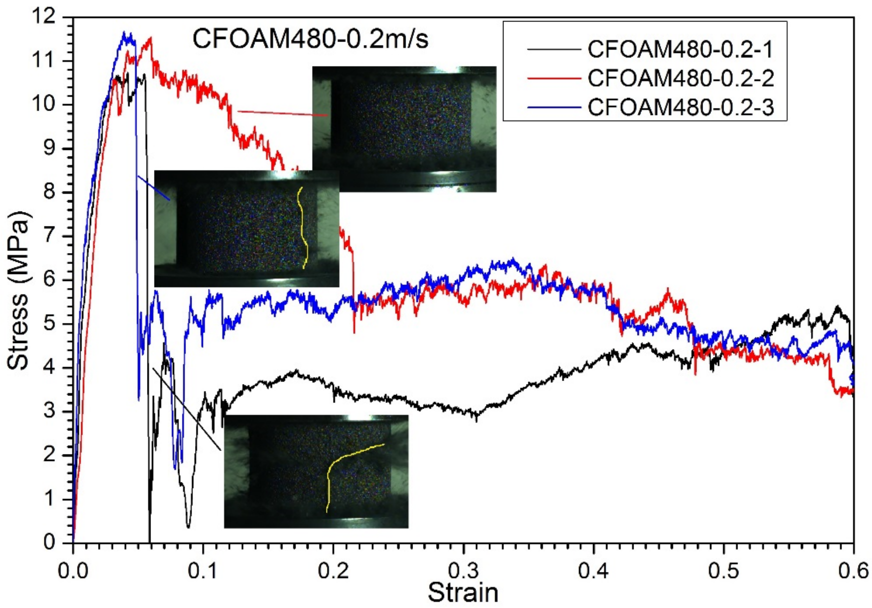

Figure 6. Long cracks lead to significant strength loss after reaching its compressive strength

The damage modes under 0.2 and 10 m/s crushing are compared for CFOAM480 as shown in Figure 7. Similar to CFOAM320, the damage modes of CFOAM480 are different under two crushing speeds. Under 0.2 m/s crushing, the damage occurs from both ends of the specimen, with a large crack observed in the longitudinal direction throughout the specimen. The middle portion of the specimen is not fragmented except the long crack appeared. CFOAM480 under

0.2 m/s crushing generates smaller fragments as compared to CFOAM320. As shown in Figure 7 (e), a large number of small particles and dust from the specimen splash away, whereas some larger pieces of CFOAM320 are shown in Figure 4 (e). The damage mode of CFOAM480 is similar to CFOAM320 under 10 m/s crushing, with the cracks initiated at the base end and propagating upwards, resulting in larger pieces of fragments from the specimen. Furthermore, more damages are located near the bottom base end instead of the top impacting end as compared to the case under 0.2 m/s crushing. The generated larger pieces of fragments under 10 m/s result in a quicker reduction of stress as compared to the lower crushing speed as shown in Figure 10.

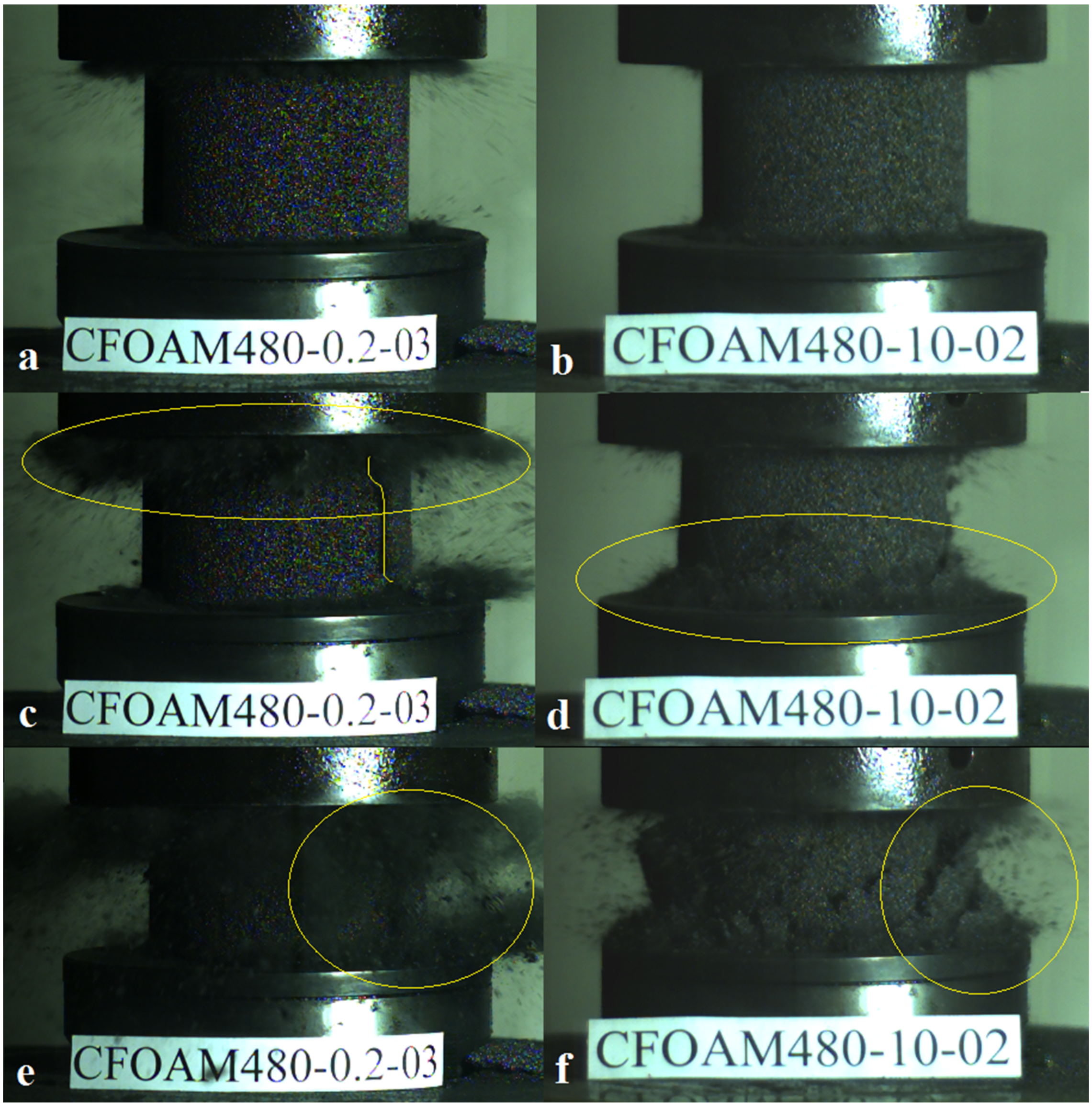

Figure 7. Damage process of carbon foam 480 at different stages under (a, c, e) 0.2 m/s and (b, d, f) 10 m/s crushing

The change of damage location for the specimens crushed under 0.2 and 10 m/s can be explained by the stress evolution theory [34, 35] as shown in Figure 8. The stress evolution in the cylinder specimen is based on the difference of the speeds of elastic and plastic stress wave, c_0 and c_1 [36]. Both speeds are calculated using equation (3), the speed of elastic wave c_0 is calculated using the elastic modulus E and the speed of plastic wave c_1 is calculated using the plastic modulus E_p. σ_y is the yield stress and it is estimated as compressive strength under quasi-static loading condition in this study, as the carbon foams show brittle failure mode with maximum compressive stress reached at small strain. V is the crushing speed of the cross-head. L is the height of specimen, t is the time since impacting and x is the distance from the bottom of the specimen. Yield stress, density, elastic and plastic modulus, and compressive strength under the respective crushing speeds are from the test data. The calculated values are given in Figure 8 (c, d).

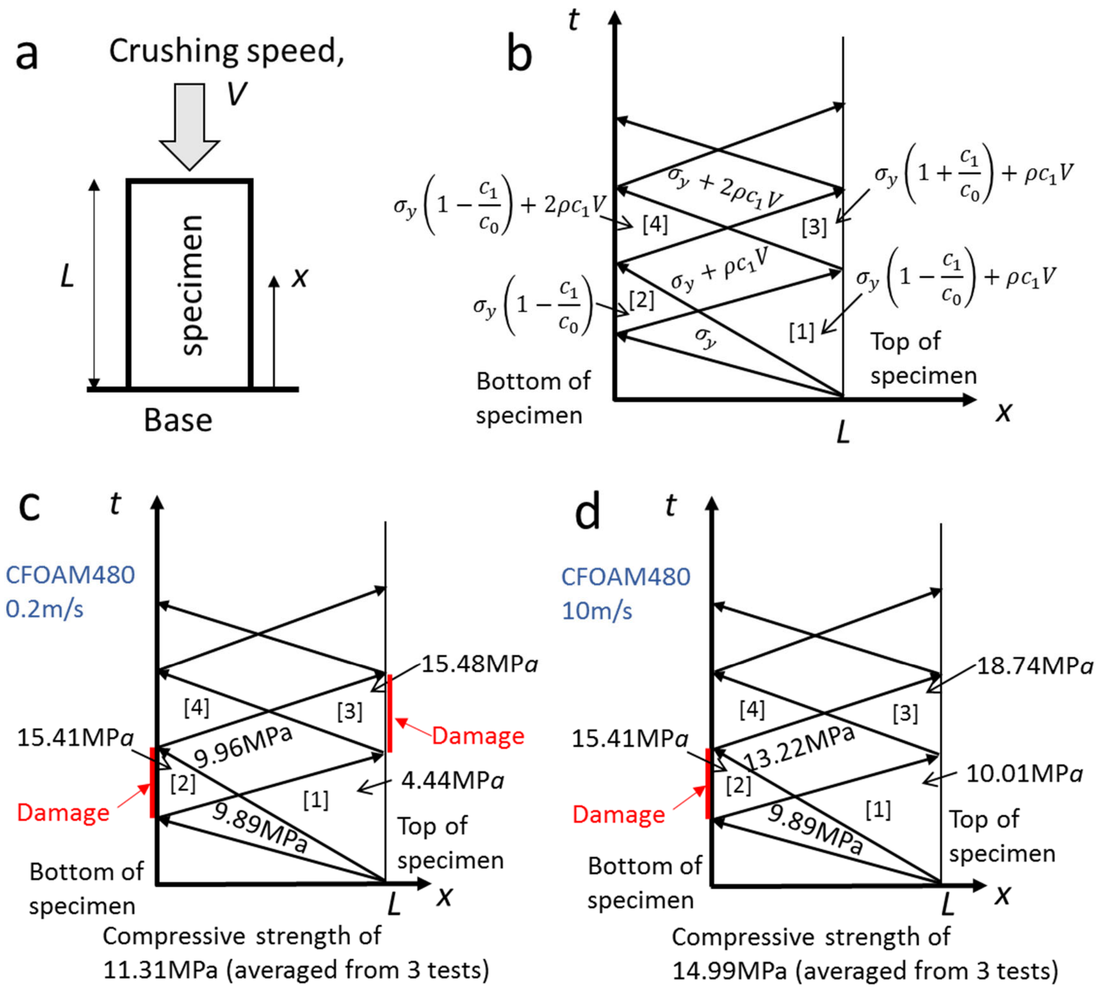

Figure 8. Schematic diagram of (a) impact on specimen; (b) stress evolution diagram under impact; (c) stress evolution of CFOAM480 under 0.2 m/s impacting; (d) stress evolution of CFOAM480 under 10 m/s impacting

As shown, the compressive strength of CFOAM480 at 0.2 and 10 m/s is different (11.31 and 14.99 MPa) due to the strain rate effect. At the instant of impact, the stresses in zone 1 of both specimens are smaller than their compressive strength, and no damage is caused at the instant of impact on the top of the specimens. The stresses of both specimens in zone 2 exceed (15.41 MPa at both speeds) the corresponding compressive strength of CFOAM480, therefore, resulting in the damage at the bottom ends for both loading cases of CFOAM480. However, the stresses at zone 3 of two loading cases are different due to different impacting velocities. The increase of stress in zone 3 compared to zone 2, indicates the vulnerability of the top portion of the specimen to damage after the damage occurs at the bottom [35]. Thus, the smaller increase in stress between zone 2 and 3 leads to a higher chance of damage initiated on the top portion of the specimen. Therefore, the damage occurs on top side of CFOAM480 under 0.2 m/s as the stress in zone 2 and 3 are similar (15.41 and 15.48 MPa) and no damage is presented on top side of CFOAM480 under 10 m/s as stress in zone 2 and 3 are quite different (15.41 and 18.74 MPa). A similar change in damage locations was observed for a type of single-phase syntactic foam under drop weight test [35]. According to this stress evolution theory, with the further increase of the impacting speed V (e.g. higher than 10 m/s), stress in zone 1 increases and may exceed the material compressive strength, and therefore may lead to the damage initiates only from the top, at the instant of impacting. Similar top propagating damage has been observed for aluminium foam material under high speed impacting [37].

4.2 Engineering stress-strain curves

4.2.1 Quasi-static and low speed crushing

Engineering stress-strain curves of two types of carbon foams under quasi-static and low speed crushing are shown in Figure 9. Elastic modulus of two carbon foams are measured using the initial slope of the stress-strain curves and are listed in Table 2. Similar trends are observed for both types of carbon foams, with a quick rise in stress at the initial stage, followed by a gradual reduction in compressive stress. The stress-strain curves are quite different from other foam materials such as EPS, PU and aluminium foams, where a rather smooth plateau stage can be observed until reaching densification with sharp rises in compressive stress [10, 11, 16, 31]. It is also different from a type of low density open-cell vitreous carbon foams which have large plateau stage in stress-strain responses [23]. The carbon foams tested in this study are brittle, with little elastic deformation and fractures occurring at the early stage near the impact end or/and the base support. The energy is mainly dissipated in the form of foam fracture and kinetic energy of flying fragments. After reaching the maximum stress, two types of stress-strain curves are shown for some test specimens. After reaching the peak stress, a gradual reduction in stress along with strain is observed for some cases while a sudden drop is presented for other cases. For instance, very similar stress-strain curves at the initial stage are shown for all specimens of CFOAM320 under 2 mm/min quasi-static crushing. However, for test 04 in Figure 9 (a), a sudden drop in stress can be observed at around 0.17 strain, which is caused by one or multiple large longitudinal cracks propagating throughout the specimen.

Foam type	CFOAM320					CFOAM480				
Test number	1	2	3	4	Ave	1	2	3	4	Ave
Elastic modulus (MPa)	333.3	432.7	392.0	394.7	388.2	807.5	832.4	801.3	855.3	824.1

Table 2. The measured elastic modulus of carbon foams under quasi-static loading condition (2 mm/min)

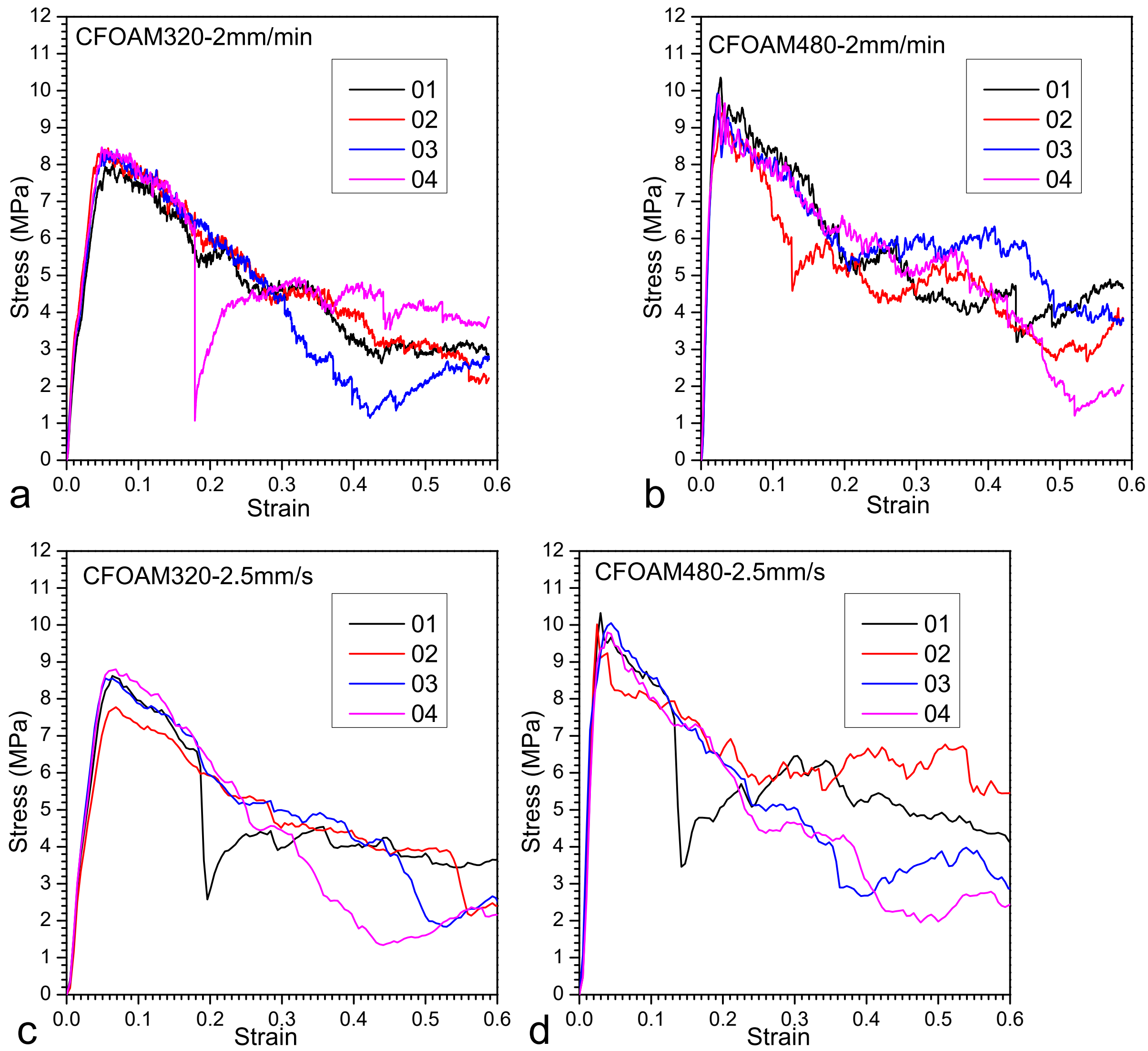

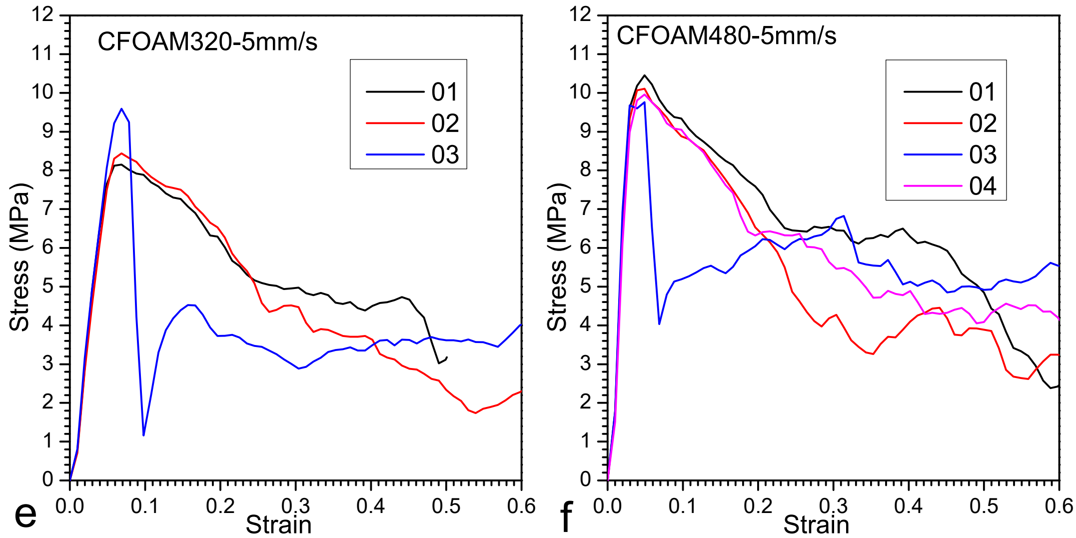

Figure 9. Engineering stress-strain curves of two carbon foams under quasi-static and low speed impact

4.2.2 Intermediate speed crushing

The engineering stress-strain curves of the two carbon foams under dynamic loading are shown in Figure 10 with the impacting speed varying from 0.2 m/s and 10 m/s. The general trends of stress-strain curves of these two carbon foams under dynamic loading are similar to those under quasi-static and low speed crushing. The stress rises sharply at the beginning, followed by either gradual reduction or a sudden drop in stress, after reaching the peak stress. With the increasing crushing speed, the occurrence of failure becomes earlier, as the strain at peak stress reduces with the higher crushing speeds. This leads to the increases in initial slopes of the stress-strain curves as well as the modulus under higher crushing speeds. Furthermore, under the higher impacting speed of 10 m/s, the gradual reduction in stress becomes faster after reaching the peak stress. For instance, under 2 mm/min crushing, the stress reduces to half of the maximum stress at strain about 0.2 and 0.3 as shown Figure 9 (b), whereas the stress reduces to half of the maximum stress at strain about 0.1 and 0.2 under 10 m/s crushing as shown in Figure 10 (d) for CFOAM480-10-02. This quicker reduction in stress under higher speed is caused by the changed damage mode, where more cracks propagate from the bottom and the larger portion of the specimen is damaged under higher impacting speed as shown in Figure 5 from section 4.1.

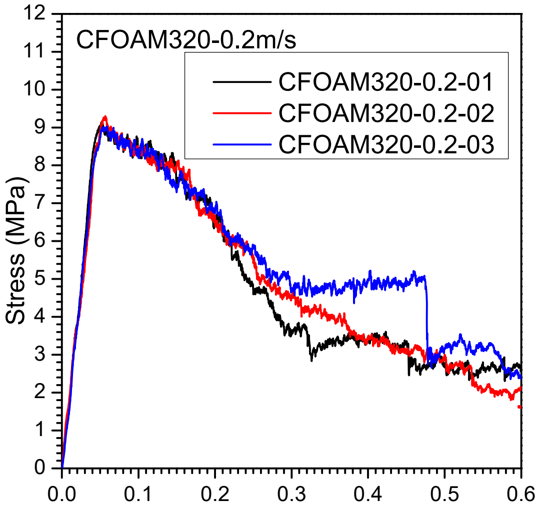
CFOAM320-0.2m/s
CFOAM320-0.2-01
CFOAM320-0.2-02
CFOAM320-0.2-03
Stress (MPa)
Strain
a

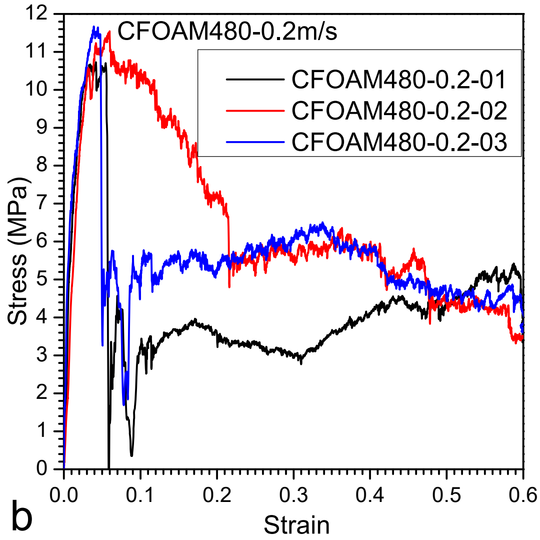
CFOAM480-0.2m/s
CFOAM480-0.2-01
CFOAM480-0.2-02
CFOAM480-0.2-03
Stress (MPa)
Strain
b

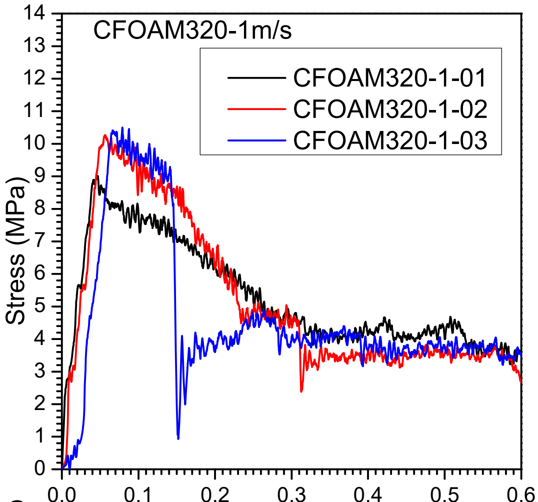
CFOAM320-1m/s
CFOAM320-1-01
CFOAM320-1-02
CFOAM320-1-03
Stress (MPa)
Strain
c

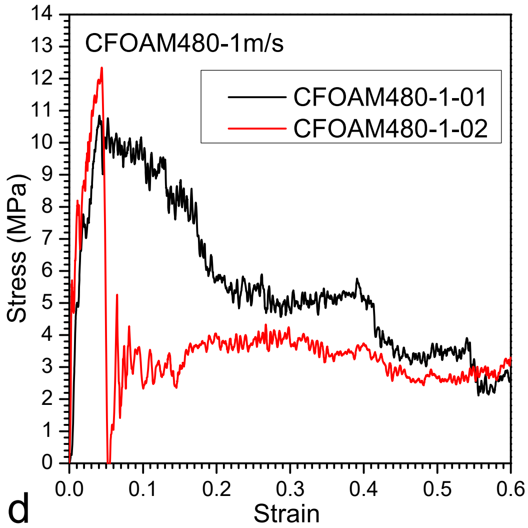
CFOAM480-1m/s
CFOAM480-1-01
CFOAM480-1-02
Stress (MPa)
Strain
d

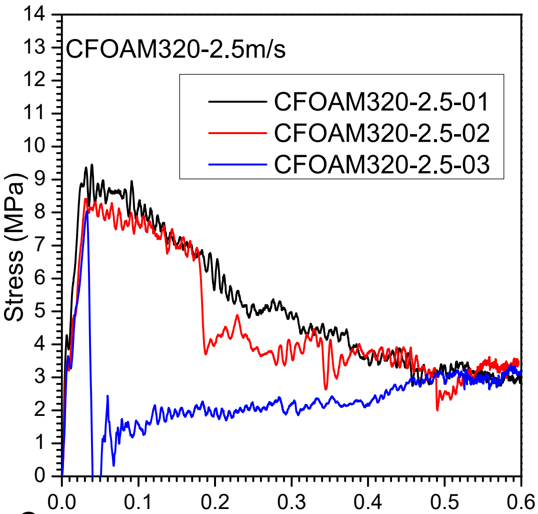
CFOAM320-2.5m/s
CFOAM320-2.5-01
CFOAM320-2.5-02
CFOAM320-2.5-03
Stress (MPa)
Strain
e

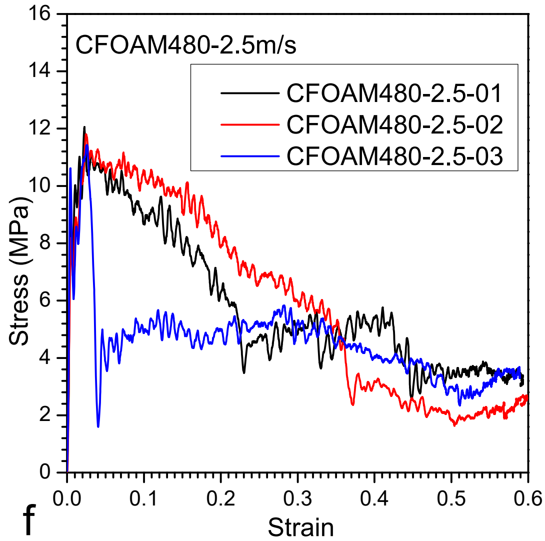
CFOAM480-2.5m/s
CFOAM480-2.5-01
CFOAM480-2.5-02
CFOAM480-2.5-03
Stress (MPa)
Strain
f

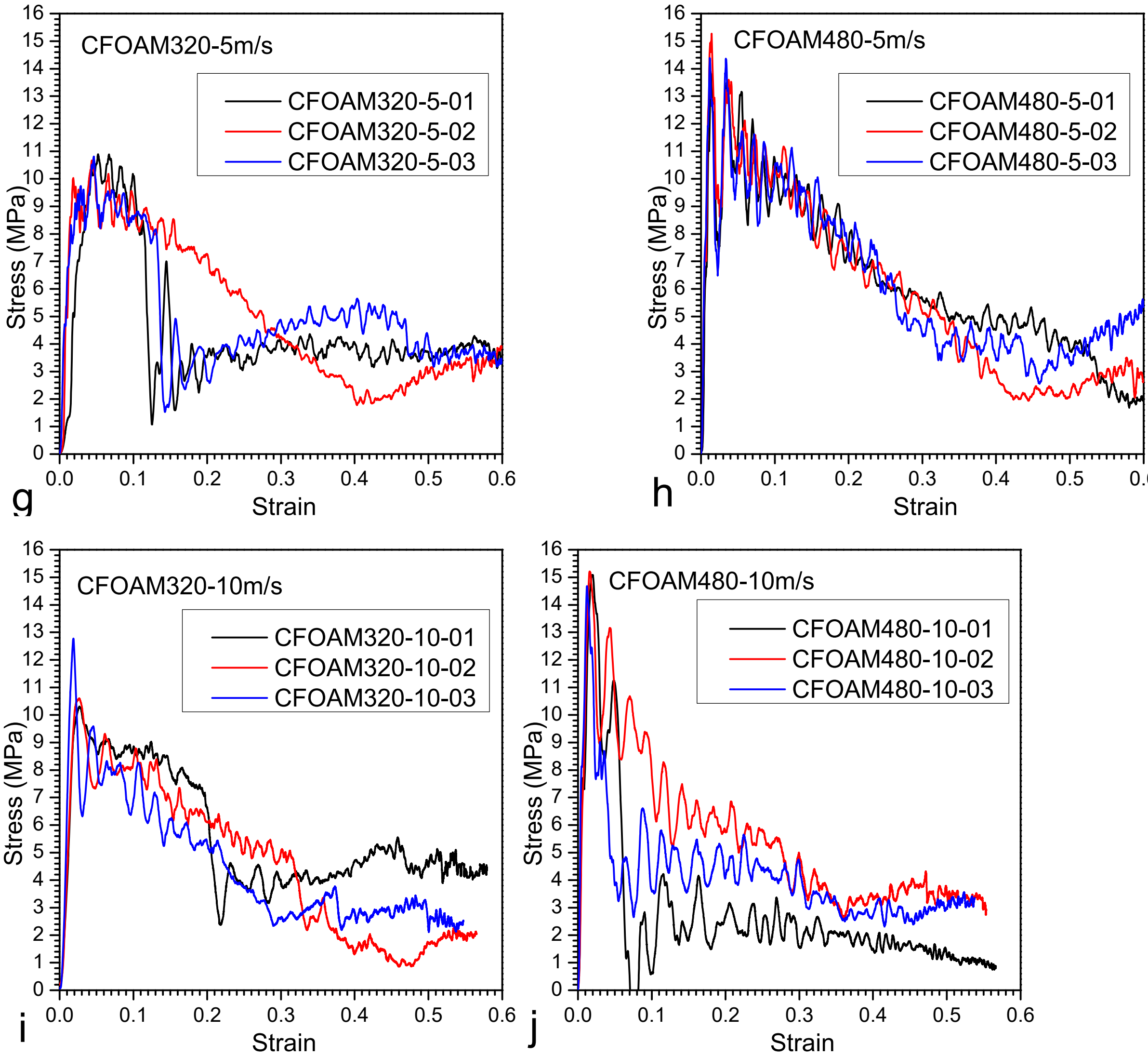

Figure 10. Engineering stress-strain curves of two carbon foams under 0.2, 1, 2.5, 5 and 10 m/s crushing

4.2.3 Stress equilibrium check for dynamic loading

As discussed in section 3.3, the stress equilibrium should be checked for material tests under dynamic loadings. The measured initial elastic modulus is 388.2 MPa for CFOAM320, which is averaged from four tests of quasi-static loading case, and 824.1 MPa for CFOAM480. The measured densities of these two carbon foams are 371 and 432 kg/m^3. The stress wave travelling speed inside carbon foam specimens can be estimated by substituting these two parameters in equation (3). The calculated travelling speeds of stress wave are 1023 and 1381 m/s for CFOAM320 and CFOAM480, respectively. As reported, three full back and forth reflections of stress wave before failure are required to reach dynamic stress equilibrium in the Split Hopkinson Pressure Bar (SHPB) test [32, 33]. Therefore, the calculated time for ensuring stress wave equilibrium is 0.293 ms and 0.217 ms for CFOAM320 and CFOAM480 respectively, giving three full back and forth traveling of stress wave within the 50 mm-high specimens. The calculated time for achieving stress wave equilibrium is then compared with the time of reaching peak stress from dynamic experiments, as listed in Table 3. Stress equilibrium is achieved for both types of specimens under quasi-static and low speed crushing tests. Under 5 m/s crushing, stress equilibrium is achieved for all three tests of CFOAM320 but not for CFOAM480. Under 10 m/s crushing, the peak stress occurs slightly earlier than three full cycles of stress wave propagation inside the specimen, therefore, stress equilibrium is not achieved for both carbon foams. However, the data under 10 m/s is also incorporated into the analysis.

Crushing speed (m/s)	CFOAM320					CFOAM480				
	Time required (ms)	Time at maximum stress (ms)			Stress equilibrium satisfied (Y/N)	Time required (ms)	Time at maximum stress (ms)			Stress equilibrium satisfied (Y/N)
		Test 1	Test 2	Test 3			Test 1	Test 2	Test 3	
2.5		1.058	0.906	0.704	Y		0.802	0.845	0.872	Y
5	0.293	0.547	0.462	0.468	Y	0.217	0.125	0.130	0.112	N
10		0.174	0.161	0.159	N		0.109	0.111	0.092	N

Table 3. Comparisons for stress equilibrium in dynamic testings

4.2.4 Summary of stress-strain curves

Engineering stress-strain curves are compared as shown in Figure 11, with one representative curve selected from each loading case. All curves have similar trend and a brittle failure response with a sharp increase in stress at the initial stage and reduction after reaching peak stress. In some cases, a sudden drop in crushing resistance is shown due to long crack initiating and propagating through the specimen. With the higher crushing speed, the slope increases for both carbon foams, indicating strain rate sensitivity of modulus. The peak stress increases with the rising crushing speeds, and CFOAM480 shows a higher strain rate sensitivity of strength as a larger increment of peak stress can be observed. Overall, the mechanical properties of carbon foams tested in this study demonstrate a clear strain rate effect, where the increases in modulus and peak stress are shown with the rising crushing speeds. The DIF values of carbon foams are calculated and discussed in section 4.3.

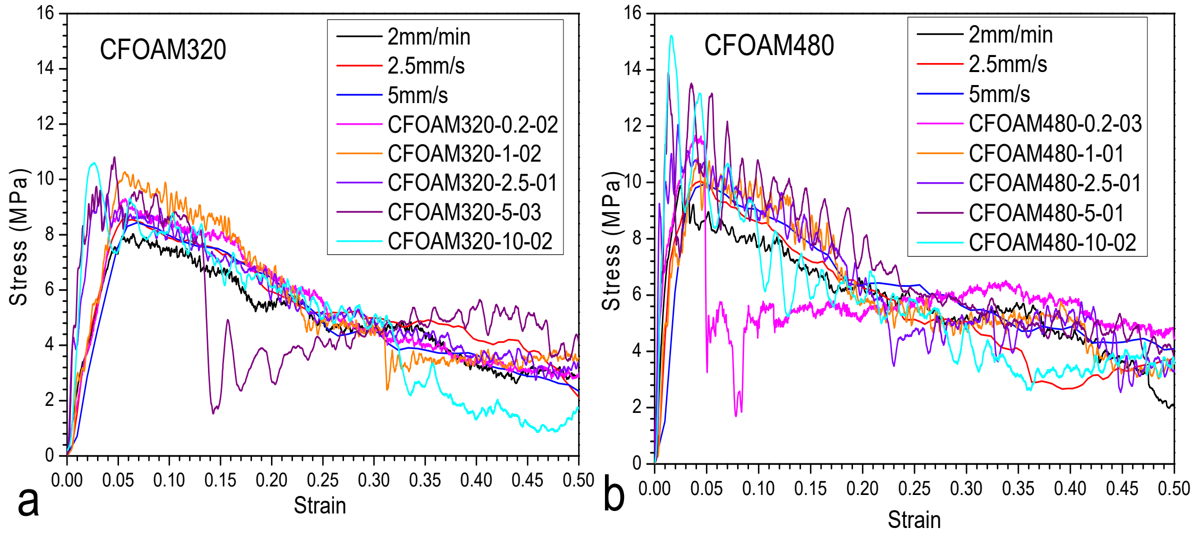

Figure 11. Representative engineering stress-strain curves of (a) CFOAM320; (b) CFOAM480 under various impacting speeds

4.3 Strain rate effect

4.3.1 Strain rate effect on compressive strength

Compressive strength of the two carbon foams under various strain rates is summarized in Table 4 and Figure 12. The compressive strength is defined as the maximum stress during the crushing. As discussed in section 3.2, the crushing speeds are not necessarily constant throughout crushing under high crushing speeds. The strain rate associated with compressive strength is therefore measured at the moment of reaching the peak stress. It is calculated using the measured instant travelling speed of cross-head at the moment of peak stress divided by the specimen height of 50 mm. It is noted that the actual strain rates are very consistent and close to the expected strain rate at the impact speeds of 2 mm/min, 2.5 mm/s, 5 mm/s, 0.2 m/s and 1 m/s. For the higher impact speeds, the average actual strain rates are less than the desired strain rates.

Carbon foam	Speed setting	Test number	Desired strain rate (s^{-1})	Actual strain rate at peak stress (s^{-1})	Compressive strength (MPa)	Secant modulus (MPa)
CFOAM320	2mm/min	01	$6.67e^{-4}$	$6.67e^{-4}$	8.03	128.1
		02		$6.67e^{-4}$	8.44	147.6
		03		$6.67e^{-4}$	8.37	136.1
		04		$6.67e^{-4}$	8.47	178.8
	2.5mm/s	01	0.05	0.05	8.62	144.3
		02		0.05	7.78	121.3
		03		0.05	8.56	171.5
		04		0.05	8.80	136.2
	5mm/s	01	0.1	0.1	8.15	130.2

		02		0.1	8.44	135.9
		03		0.1	9.59	154.4
	0.2m/s	01	4	4.3	9.13	180.6
		02		4.3	9.30	167.7
		03		4.3	9.03	157.0
	1m/s	01	20	19.9	9.02	194.0
		02		18.7	10.27	202.2
		03		19.7	10.5	206.5
	2.5m/s	01	50	42.0	9.45	250.5
		02		41.2	8.42	286.5
		03		52.9	8.04	262.7
	5m/s	01	100	79.9	10.89	293.6
		02		76.9	10.67	277.5
		03		79.8	10.80	244.2
	10m/s	01	200	150.7	10.31	421.4
		02		156.2	10.61	462.7
		03		121.1	12.77	793.7
CFOAM480	2mm/min	01	$6.67e^{-4}$	$6.67e^{-4}$	10.36	411.9
		02		$6.67e^{-4}$	9.39	343.8
		03		$6.67e^{-4}$	9.93	478.9
		04		$6.67e^{-4}$	9.88	419.9
	2.5mm/s	01	0.05	0.05	10.32	398.3
		02		0.05	10.02	415.6
		03		0.05	10.05	247.4
		04		0.05	9.80	278.3
	5mm/s	01	0.1	0.1	10.45	319.4
		02		0.1	10.11	310.9
		03		0.1	9.76	298.3
		04		0.1	9.96	306.3
	0.2m/s	01	4	4.3	10.73	341.2
		02		4.4	11.55	281.4
		03		4.3	11.67	298.6
	1m/s	01	20	19.1	10.85	293.8
		02		21.4	12.35	288.7
		03		-	-	-
	2.5m/s	01	50	39.4	12.06	581.1
		02		36.3	11.81	517.4
		03		46.3	11.43	467.8
	5m/s	01	100	73.0	13.89	1344.8
		02		72.7	15.27	1174.7
		03		72.3	14.39	1358.45
	10m/s	01	200	178.2	15.09	844.6
		02		138.1	15.21	1110.2
		03		135.8	14.68	1355.5

Table 4. Measured compressive strength and secant modulus of two carbon foams under different impacting speeds

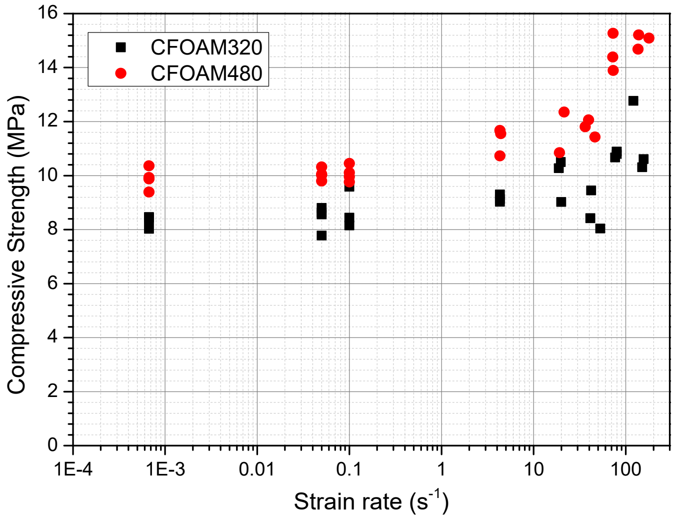

Figure 12. Compressive strength of two carbon foams at different strain rates

As shown in Figure 12, increasing trends of compressive strength with higher strain rate are shown for both carbon foams. At strain rates below 0.1 s^{-1}, a very minor increase in compressive strength is shown with the increase of strain rate. This is different from the previous study of closed-cell aluminium foam [20], in which the compressive strength (first peak) of aluminium foam increases linearly with log($\dot{\varepsilon}$) at very low strain rate from 10^{-5} to 10^{-2} s^{-1}. Compressive strength of both tested carbon foams in this study increases significantly with the rising strain rate when the strain rate is over 4 s^{-1} as shown in Figure 12. It is also observed that the compressive strength of both carbon foams can be expressed in a power relationship with strain rate, as the increases in compressive strength at higher strain rates are much greater than that at lower strain rates.

Similar power laws are observed for strain rate effect of plateau stress of closed-cell aluminium foam in the previous study [16] as mentioned in section 2.1. Therefore, a similar relationship is used for modelling the strain rate effect on compressive strength of the carbon foams as below.

$$DIF = \frac{\sigma_d}{\sigma_s} = x(1 + y\left(\frac{\dot{\varepsilon}}{\dot{\varepsilon}_0}\right)^z) \quad (4)$$

where DIF is dynamic increase factor which is the ratio of compressive strength under dynamic loading (σ_d) to that under quasi-static loading (σ_s); *x, y* and *z* are coefficients and dimensionless and $\dot{\varepsilon}_0$ (quasi-static strain rate) is 6.67×10^{-4} s^{-1} in this study for both foams. In this case, the compressive strength under static loading, σ_s is averaged from the quasi-static testing for each type of carbon foam. Strain rate is calculated using the instant crushing speed at the peak stress divided by the specimen height.

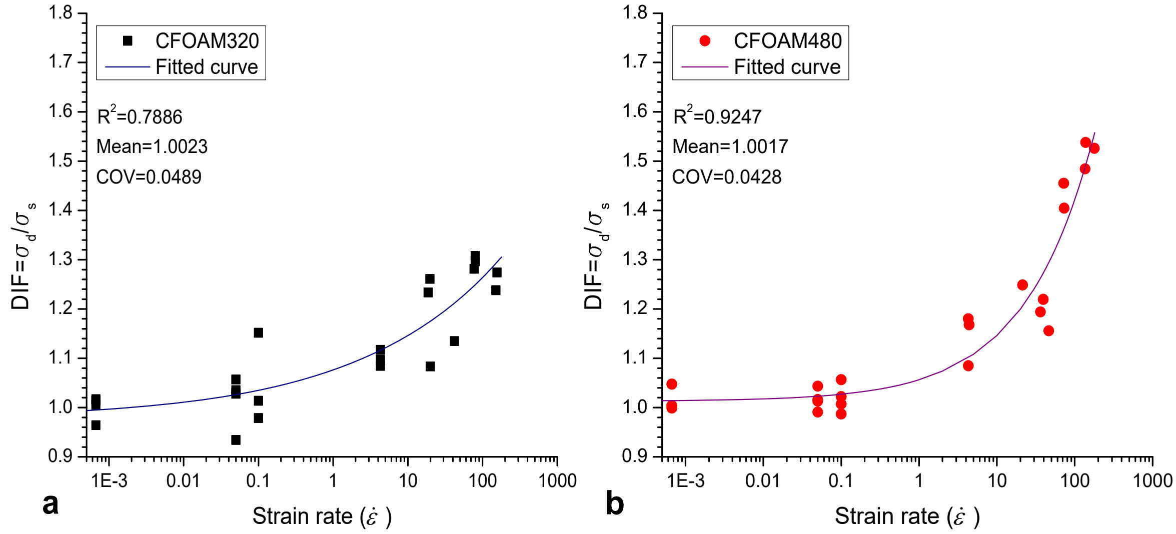

Figure 13. Dynamic increase factor of compressive strength with respect to strain rate for (a) CFOAM320; (b) CFOAM480

The measured compressive strength of carbon foams under various strain rates is fitted and shown in Figure 13. Three far-off points are removed from out of 27 tests for each type of carbon foam. The curves are well fitted with R^2 of 0.7886 and 0.9247 for CFOAM320 and CFOAM480, respectively. Values of mean and coefficient of variation (COV) are listed on the graph. Mean is the average of the ratios of the fitted DIF to the measured DIF under all strain rates, and the COV is the standard deviation of these ratios. The relationships between DIF of compressive strength and strain rate of the two carbon foams are given below.

$$\mathrm{DIF} = \frac{\sigma_d}{\sigma_s} = 0.9763(1 + 0.01903\left(\frac{\dot{\varepsilon}}{\dot{\varepsilon}_0}\right)^{0.2299}) \text{ for CFOAM320 } (10^{-4} < \dot{\varepsilon} < 156\ \mathrm{s}^{-1}) \tag{5}$$

$$\mathrm{DIF} = \frac{\sigma_d}{\sigma_s} = 1.013(1 + 0.001215\left(\frac{\dot{\varepsilon}}{\dot{\varepsilon}_0}\right)^{0.4872}) \text{ for CFOAM480 } (10^{-4} < \dot{\varepsilon} < 178\ \mathrm{s}^{-1}) \tag{6}$$

4.3.2 Strain rate effect on modulus

The modulus of the carbon foams under various loading rates is measured. The secant modulus instead of the initial modulus is selected for comparisons. As shown in Figure 14 (a), the initial modulus is the initial slope of the engineering stress versus strain of specimen, whereas the secant modulus is defined as the failure stress (maximum compressive stress) divided by the failure strain. The failure strain is taken as the strain at the failure stress. This is because in some cases, the initial slopes for the same carbon foam specimens can be different, even under the same loading rate. One example is shown in Figure 14 (b), the initial slopes of three specimens are quite different, even though the failure stress and failure strain are similar among the three tests. These initial discrepancies in stress-strain curves could be caused by many factors, including slight differences in dimension, density, microstructure, and surface flatness among specimens.

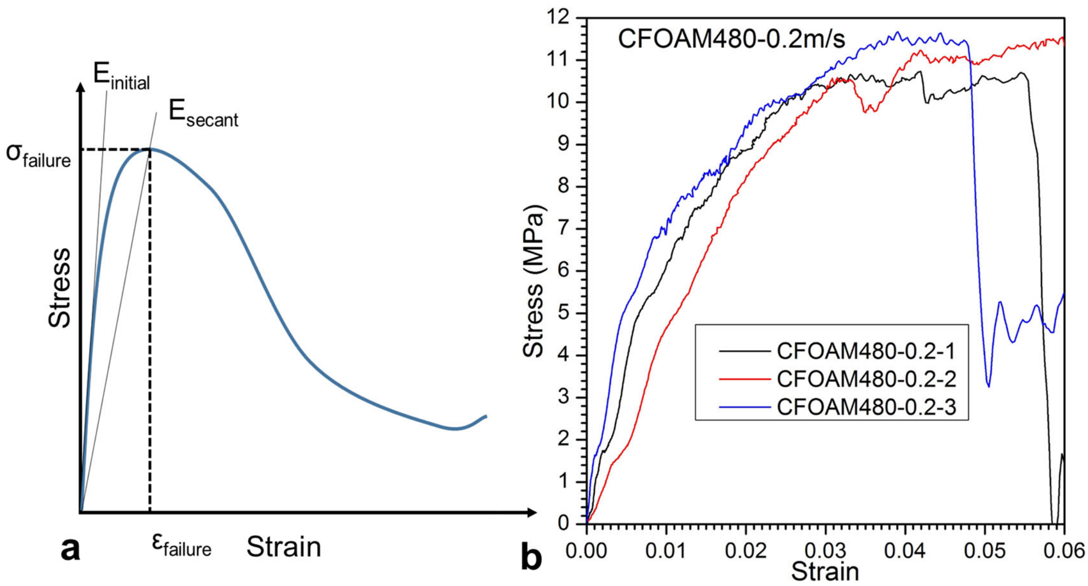

Figure 14. (a) Definition of initial and secant modulus; (b) example of discrepancies of stress-strain curves in the initial stage for the same type of carbon foam under the same loading rate

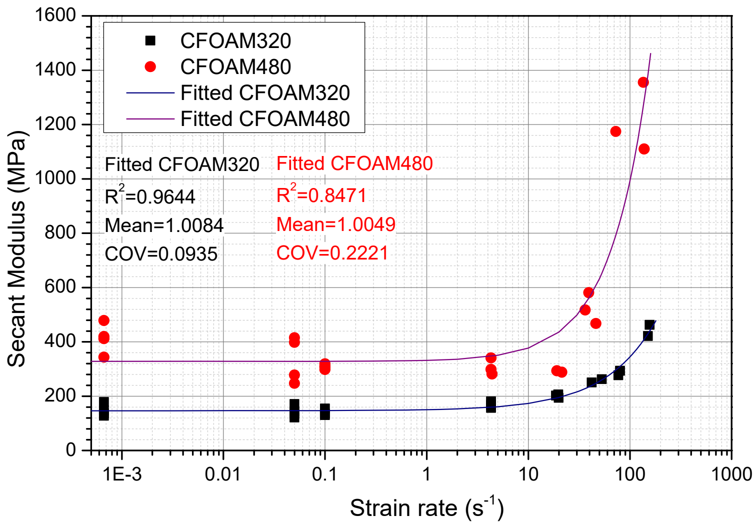

Figure 15. Secant modulus of two carbon foams under different strain rates

The secant modulus of the two carbon foams under various loading rates is listed in Table 4. The fitted curves of both carbon foams are shown in Figure 15 with three far-off points removed for each carbon foam. The secant modulus measured under the same loading rate varies, especially for CFOAM480. It might be caused by the interaction of stress wave propagation inside specimen as stress equilibrium is not reached for several cases under high loading rates. In general, increasing trends can be observed for both carbon foams with the increase in strain rate. CFOAM480 has a larger increment of secant modulus than CFOAM320 with the increase in strain rate. This is consistent with aluminium foam materials [16, 38], as the material properties of foam materials are in power relationship with both strain rate and density. In other words, the denser foam shows more significant strain rate sensitivity on their compressive and plateau stresses.

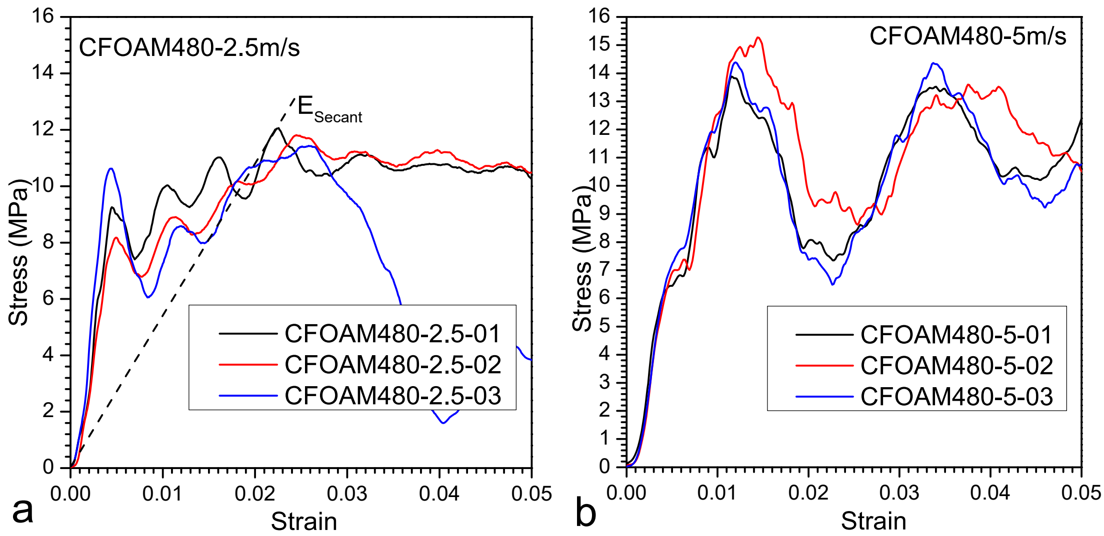

Figure 16. Early stage of stress-strain curves of CFOAM480 under (a) 2.5 and (b) 5m/s crushing

The secant modulus measured from all tests is shown in Figure 15. CFOAM320 shows similar power relationship between modulus and strain rate as compared to the strain rate effect of compressive strength. CFOAM480, however, shows some inconsistent changes in modulus with respect to strain rate, even though the general trend of modulus increases with the strain rate as well. For instance, from quasi-static to low speed crushing up to around 20 s^{-1}, the secant modulus decreases slightly with the increase of strain rate and high value of secant modulus can be observed under the strain rate around 80 s^{-1}. These can be explained by the stress-strain curves at very early stages of CFOAM480 under dynamic loading. For instance, engineering stress-strain curves of CFOAM480 under 2.5 and 5 m/s crushing are compared in Figure 16. Under 2.5 m/s, the maximum stress is reached after the first peak, whereas for 5 m/s crushing, the maximum stress occurs at the first peak. Therefore, the strain at the peak stress of CFOAM480 under 5 m/s is almost half of that under 2.5 m/s, resulting in a significant increase of secant modulus from around 500 MPa to more than 1300 MPa when crushing speed is increased from 2.5 to 5 m/s, although the failure stress is similar under the two loading rates.

$$E_{\text{secant}} = 146.8(1+3.95\times10^{-5}\left(\frac{\dot{\varepsilon}}{\dot{\varepsilon}_0}\right)^{0.8759}) \text{ for CFOAM320 } (10^{-4} < \dot{\varepsilon} < 156 \text{ s}^{-1}) \quad (7)$$

$$E_{\text{secant}} = 328.3(1+2.841\times10^{-6}\left(\frac{\dot{\varepsilon}}{\dot{\varepsilon}_0}\right)^{1.131}) \text{ for CFOAM480 } (10^{-4} < \dot{\varepsilon} < 178 \text{ s}^{-1}) \quad (8)$$

where E_{secant} is the secant modulus.

4.4 Comparison of mechanical properties

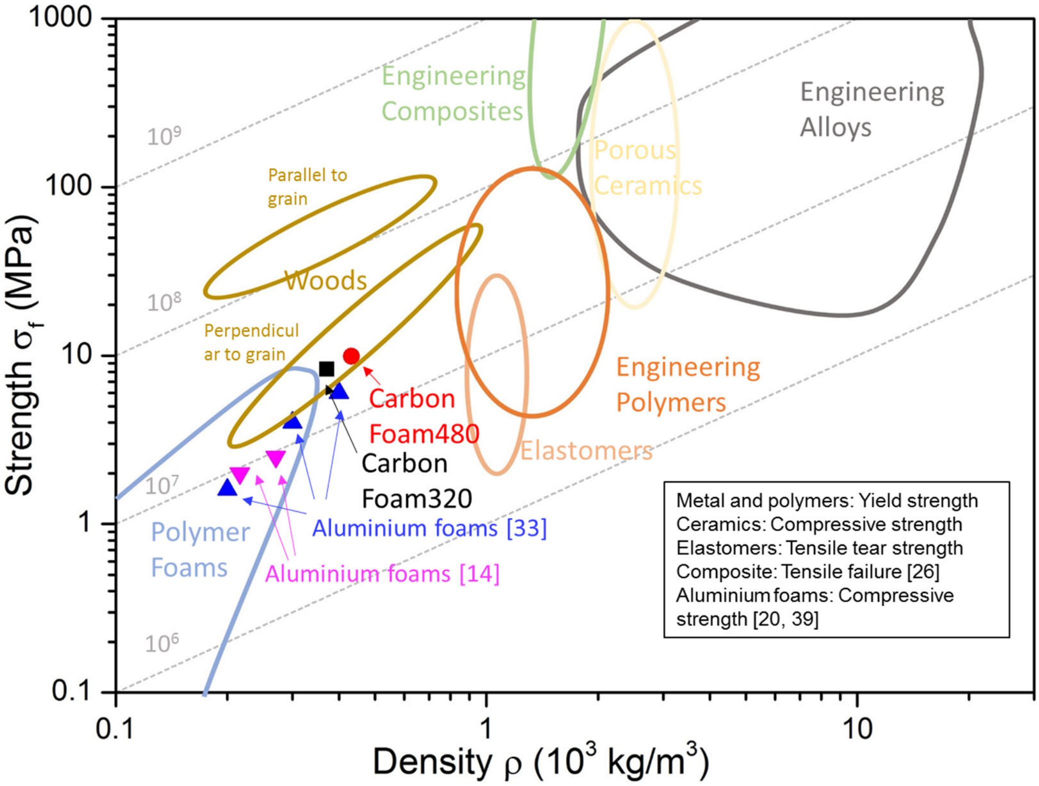

Figure 17. Ashby chart of density and strength of materials [20, 26, 39]; Note: for carbon foams strength refers to the measured compressive strength. Dash lines indicate the contours of constant strength-density ratio c=$\frac{\sigma_f}{\rho}$

The averaged compressive strength of carbon foams measured under quasi-static loading condition are 8.33 MPa and 9.89 MPa, for CFOAM320 and CFOAM480, respectively. Their averaged elastic moduli are 388.2 MPa and 824.1 MPa for CFOAM320 and CFOAM480 under the same quasi-static loading condition. The compressive strength of carbon foams is marked out against their densities in an Ashby chart and compared with other materials, as shown in Figure 17 [20, 26, 39]. With the averaged densities of 371 and 432 kg/m^3, carbon foam has similar mechanical properties to woods and wood products, in terms of compressive strength and densities. As indicated by the contour lines, the strength-density ratio of carbon foams is lower than many of the engineering alloys, ceramics and composites. However, the compressive strength of carbon foam is higher than aluminium foams with similar densities. Furthermore, due to the advantages such as low thermal conductivity, high operational temperature and corrosion resistant [24], carbon foams can be used in these extreme conditions where conventional engineering alloys and composite cannot withstand. The operational temperature for composites and polymers is often less than 100 degree Celsius [40], whereas the operational temperature for carbon foams can reach 600 degree Celsius in the air [24].

5 Conclusion

Mechanical properties of two densities of carbon foams, CFOAM320 and CFOAM480 are tested and measured under various loading rates ranging from 6.67×10^{-4} to 178 s^{-1}. Different from other foam materials such as aluminium foams, EPS foams and PU foams, two densities of carbon foams experience brittle failure mode under various loading rates, with the maximum stress achieved at small strain value of less than 0.05. Two types of stress-strain curves and damage modes can be seen for both carbon foams. A gradual reduction in stress or a sudden drop in stress can be observed after reaching the peak stress. This gradual reduction in stress is caused by cracking near the interfaces of the specimen and flying-off pieces from the specimen, whereas the sudden drop in stress is due to the large longitudinal cracks throughout the specimens. Both damage modes occur randomly under all loading cases. Significant strain rate effect is observed for both carbon foams. The increase in compressive strength is more significant under higher strain rates and the carbon foam with higher density. The dynamic DIF values are calculated and compared for the two carbon foams. Empirical formulae of the mechanical properties such as compressive strength and modulus with respect to strain rate are derived from the testing data.

Acknowledgements

The authors acknowledge the support from the Australian Research Council via Discovery Early Career Researcher Award (DE160101116). The authors acknowledge the assistance provided by Mr Zhixing Li from Curtin University for testing preparations.

References

[1] G.J. McShane, D.D. Radford, V.S. Deshpande, N.A. Fleck, The response of clamped sandwich plates with lattice cores subjected to shock loading, European Journal of Mechanics - A/Solids, 25 (2006) 215-229.

[2] Z. Ozdemir, E. Hernandez-Nava, A. Tyas, J.A. Warren, S.D. Fay, R. Goodall, I. Todd, H. Askes, Energy absorption in lattice structures in dynamics: Experiments, International Journal of Impact Engineering, 89 (2016) 49-61.

[3] X. Wu, K. Xiao, Q. Yin, F. Zhong, C. Huang, Experimental study on dynamic compressive behaviour of sandwich panel with shear thickening fluid filled pyramidal lattice truss core, International Journal of Mechanical Sciences, 138-139 (2018) 467-475.

[4] L. Aktay, A.K. Toksoy, M. Güden, Quasi-static axial crushing of extruded polystyrene foam-filled thin-walled aluminum tubes: Experimental and numerical analysis, Materials & Design, 27 (2006) 556-565.

[5] Z. Wang, J. Liu, Z. Lu, D. Hui, Mechanical behavior of composited structure filled with tandem honeycombs, Composites Part B: Engineering, 114 (2017) 128-138.

[6] J. Zhang, M. Ashby, The out-of-plane properties of honeycombs, International Journal of Mechanical Sciences, 34 (1992) 475-489.

[7] P.-B. Su, B. Han, M. Yang, Z.-H. Wei, Z.-Y. Zhao, Q.-C. Zhang, Q. Zhang, K.-K. Qin, T.J. Lu, Axial compressive collapse of ultralight corrugated sandwich cylindrical shells, Materials & Design, 160 (2018) 325-337.

[8] C. Kılıçaslan, M. Güden, İ.K. Odacı, A. Taşdemirci, Experimental and numerical studies on the quasi-static and dynamic crushing responses of multi-layer trapezoidal aluminum corrugated sandwiches, Thin-Walled Structures, 78 (2014) 70-78.

[9] M.F. Ashby, A. Evans, N.A. Fleck, L.J. Gibson, J.W. Hutchinson, H.N.G. Wadley, Metal foams: a design guide, Materials & Design, 23 (2002) 119.

[10] W. Chen, H. Hao, D. Hughes, Y. Shi, J. Cui, Z.-X. Li, Static and dynamic mechanical properties of expanded polystyrene, Materials & Design, 69 (2015) 170-180.

[11] S. Ouellet, D. Cronin, M. Worswick, Compressive response of polymeric foams under quasi-static, medium and high strain rate conditions, Polymer Testing, 25 (2006) 731-743.

[12] N. Gupta, E. Woldesenbet, P. Mensah, Compression properties of syntactic foams: effect of cenosphere radius ratio and specimen aspect ratio, Composites Part A: Applied Science and Manufacturing, 35 (2004) 103-111.

[13] I.N. Orbulov, J. Ginsztler, Compressive characteristics of metal matrix syntactic foams, Composites Part A: Applied Science and Manufacturing, 43 (2012) 553-561.

[14] T. Fiedler, M. Taherishargh, L. Krstulović-Opara, M. Vesenjak, Dynamic compressive loading of expanded perlite/aluminum syntactic foam, Materials Science and Engineering: A, 626 (2015) 296-304.

[15] L. Peroni, M. Scapin, C. Fichera, D. Lehmhus, J. Weise, J. Baumeister, M. Avalle, Investigation of the mechanical behaviour of AISI 316L stainless steel syntactic foams at different strain-rates, Composites Part B: Engineering, 66 (2014) 430-442.

[16] D. Ruan, G. Lu, F. Chen, E. Siores, Compressive behaviour of aluminium foams at low and medium strain rates, Composite Structures, 57 (2002) 331-336.

[17] R. Huang, S. Ma, M. Zhang, J. Xu, Z. Wang, Dynamic deformation and failure process of quasi-closed-cell aluminum foam manufactured by direct foaming technique, Materials Science and Engineering: A, (2019).

[18] G. Lu, T. Yu, Energy Absorption of Structures and Materials, Woodhead publishing limited, Cambridge England, 2003.

[19] X. Zhang, G. Cheng, A comparative study of energy absorption characteristics of foam-filled and multi-cell square columns, International Journal of Impact Engineering, 34 (2007) 1739-1752.

[20] A. Paul, U. Ramamurty, Strain rate sensitivity of a closed-cell aluminum foam, Materials Science and Engineering: A, 281 (2000) 1-7.

[21] F. Moglie, D. Micheli, S. Laurenzi, M. Marchetti, V. Mariani Primiani, Electromagnetic shielding performance of carbon foams, Carbon, 50 (2012) 1972-1980.

[22] M. Grujicic, B. Pandurangan, C.L. Zhao, S.B. Biggers, D.R. Morgan, Hypervelocity impact resistance of reinforced carbon–carbon/carbon–foam thermal protection systems, Applied Surface Science, 252 (2006) 5035-5050.

[23] M. Letellier, C. Delgado-Sanchez, M. Khelifa, V. Fierro, A. Celzard, Mechanical properties of model vitreous carbon foams, Carbon, 116 (2017) 562-571.

[24] D.M. Spradling, R.A. Guth, Carbon foams, Advanced materials & processes, 161 (2003) 29-31.

[25] E. Andrews, G. Gioux, P. Onck, L. Gibson, Size effects in ductile cellular solids. Part II: experimental results, International Journal of Mechanical Sciences, 43 (2001) 701-713.

[26] L.J. Gibson, M.F. Ashby, Cellular solids: structure and properties, Cambridge university press, 1999.

[27] J. Shen, G. Lu, D. Ruan, Compressive behaviour of closed-cell aluminium foams at high strain rates, Composites Part B: Engineering, 41 (2010) 678-685.

[28] J. Klett, R. Hardy, E. Romine, C. Walls, T. Burchell, High-thermal-conductivity, mesophase-pitch-derived carbon foams: effect of precursor on structure and properties, Carbon, 38 (2000) 953-973.

[29] T. Nieh, K. Higashi, J. Wadsworth, Effect of cell morphology on the compressive properties of open-cell aluminum foams, Materials Science and Engineering: A, 283 (2000) 105-110.

[30] P. Onck, E. Andrews, L. Gibson, Size effects in ductile cellular solids. Part I: modeling, International Journal of Mechanical Sciences, 43 (2001) 681-699.

[31] B. Jiang, Z. Wang, N. Zhao, Effect of pore size and relative density on the mechanical properties of open cell aluminum foams, Scripta Materialia, 56 (2007) 169-172.

[32] K.S. Vecchio, F. Jiang, Improved Pulse Shaping to Achieve Constant Strain Rate and Stress Equilibrium in Split-Hopkinson Pressure Bar Testing, Metallurgical and Materials Transactions A, 38 (2007) 2655-2665.

[33] W. Chen, Q. Meng, H. Hao, J. Cui, Y. Shi. Quasi-static and dynamic tensile properties of fiberglass/epoxy laminate sheet, Construction and building material, 143 (2017) 247-258.

[34] W. Johnson, Impact Strength of Materials, London: Edward Arnold (Publishers) Limited, (1972).

[35] T.M. Pham, W. Chen, J. Kingston, H. Hao, Impact response and energy absorption of single phase syntactic foam, Composites Part B: Engineering, 150 (2018) 226-233.

[36] T. Yu, X. Qiu, Introduction to impact dynamics, John Wiley & Sons, 2018.

[37] M.A. Kader, M.A. Islam, P.J. Hazell, J.P. Escobedo, M. Saadatfar, A.D. Brown, G.J. Appleby-Thomas, Modelling and characterization of cell collapse in aluminium foams during dynamic loading, International Journal of Impact Engineering, 96 (2016) 78-88.

[38] P.J. Tan, J.J. Harrigan, S.R. Reid, Inertia effects in uniaxial dynamic compression of a closed cell aluminium alloy foam, Materials science and technology, 18 (2002) 480-488.

[39] CYMAT, Technical Manual for CYMAT SmartMetal™, CYMAT Technologies Ltd, (2009) 5-1-17.

[40] H. Le Ferrand, Robotics: Science preceding science fiction, MRS Bulletin, 44 (2019) 295-301.